J꠸M PAPERS

A unifying theory of jet screech

Daniel Edgington-Mitchell[1,†], **Xiangru Li**[2], **Nianhua Liu**[2], **Feng He**[2], **Tsz Yeung Wong**[1], **Jacob Mackenzie**[1] **and Petronio Nogueira**[1]

[1]Department of Mechanical and Aerospace Engineering, Monash University, Melbourne, VIC 3800, Australia

[2]Department of Engineering Mechanics, Tsinghua University, Beijing 100084, PR China

This paper describes the mechanism underpinning modal staging behaviour in screeching jets. An upstream-propagating subsonic guided-jet mode is shown to be active in all stages of screech. Axial variation of shock-cell spacing manifests in the spectral domain as a series of suboptimal peaks. It is demonstrated that the guided-jet mode may be energized by interactions of the Kelvin–Helmholtz wavepacket with not only the primary shock wavenumber peak, but also suboptimal peaks; interaction with suboptimals is shown to be responsible for closing the resonance loop in multiple stages of jet screech. A consideration of the full spectral representation of the shocks reconciles several of the classical models and results for jet screech that had heretofore been paradoxical. It is demonstrated that there are multiple standing waves present in the near field of screeching jets, corresponding to the superposition of the various waves active in these jets. Multimodal behaviour is explored for jets in a range of conditions, demonstrating that multiple peaks in the frequency spectra can be due to either changes in which peak of the shock spectra the Kelvin–Helmholtz wavepacket is interacting with, or a change in azimuthal mode, or both. The absence of modal staging in high-aspect-ratio non-axisymmetric jets is also explained in the context of the aforementioned mechanism. The paper closes with a new proposed theory for frequency selection in screeching jets, based on the observation that these triadic interactions appear to underpin selection of the guided-jet mode wavelength in all measured cases.

Key words: jet noise, aeroacoustics, shock waves

† Email address for correspondence: daniel.mitchell@monash.edu

1. Introduction

The discrete-frequency high-amplitude tones known as screech were first detected in the acoustic field of off-design supersonic jets by Powell (1953). A distinctive property of screech tones is their propensity to exhibit discontinuous changes in frequency with only minor changes in jet supply pressure. These abrupt changes in frequency are referred to as a modal 'staging'; stage jumps are often observed to correspond to changes in the dominant azimuthal mode of the jet (Davies & Oldfield 1962). Despite recent progress in understanding jet screech (Edgington-Mitchell 2019), a number of open questions remain, with the mechanism of modal staging amongst the most tantalizing. The lack of clarity on mode staging is symptomatic of broader disagreements regarding the physics governing the screech cycle; there are several competing theories with seemingly irreconcilable differences in their fundamental construction that yield identical frequency predictions. Powell (1953) suggested the first such model, based on equispaced monopoles, with the frequency of the screech selected to maximize directivity of the fundamental in the upstream direction, and the harmonic at $90°$. Tam, Seiner & Yu (1986) proposed what they termed the 'weakest-link model', considering screech to be the upstream limit of broadband shock-associated noise, with the upstream-propagating component the weakest link of the resonance loop. From this dissimilar approach they arrived at the same expression; (1.1) can be constructed on either basis:

$$f_s = \frac{U_c k_S}{2\pi(1 + M_c)}.$$ (1.1)

Here f_s is the screech frequency, M_c is the convective Mach number, U_c is the convection velocity and k_S is the wavenumber of the shock cells. In the approach of Tam and co-authors the screech tones arise due to interaction between a stationary wave of wavenumber k_S and a convecting instability wave with phase velocity U_c. Despite their different bases, the predictions arrived at by the two theories are identical. It should, however, be noted that in Tam *et al.* (1986) k_S is written as $k_n; n = 1, 2, 3, \ldots$; a full representation of the shock cell structure requires an infinite number of modes, whereas Powell's original formulation was only based on a fixed spacing. However, in Tam *et al.* (1986) and the body of work that followed, it was typically assumed that higher-order shock cell modes could be neglected, thus returning to an equivalence in the application of the two models.

Equation (1.1) can produce accurate predictions of screech frequency for some jet operating conditions; however, it is unable to account for the modal staging behaviour of jet screech, as neither the convection velocity nor the shock spacing has been observed to change in a discontinuous manner with changes in operating condition (Clem, Zaman & Fagan 2016; Mercier, Castelain & Bailly 2017).

The limitations of (1.1) have motivated a number of alternative approaches to both understanding and predicting jet screech. One such attempt was grounded in an investigation of the standing wave in the near field of screeching jets first described in the work of Westley & Woolley (1975). Panda (1999) demonstrated that a standing wave would form as per (1.2):

$$k_{sw} = k_u + k_d,$$ (1.2)

where k_u, k_d and k_{sw} are the wavenumbers of the upstream-propagating waves, the downstream-propagating waves and the standing wave, respectively. On this basis, since

$k_u = \omega_s/u_u$ and $k_d = \omega_s/u_d$, where u is the phase velocity of the wave, (1.2) can be rewritten in its original form (left) which assumes that the upstream-propagating wave is acoustic, or in a more general form with phase velocity for waves propagating upstream denoted u_u and downstream denoted u_d (right):

$$f_s = \frac{U_c k_{sw}}{2\pi(1 + M_c)} \quad \text{or} \quad f_s = \frac{u_d k_{sw}}{2\pi(1 + u_d/u_u)}. \tag{1.3a,b}$$

Panda (1999) suggested that since predictions on the basis of (1.3a,b) were more robust than (1.1), the standing wave might be a more appropriate length scale for screeching jets than the shock-cell spacing. However at least in a simplified framework that assumes constant wave velocities (which is also an assumption in both models that lead to (1.1)), (1.3a,b) is essentially mathematically exact rather than being a model; while valuable in understanding the structure of screeching jets, the equation itself has no predictive power and cannot explain staging.

If we maintain the assumption of constant wave velocities, it is apparent that for both (1.1) and (1.3a,b) to be valid requires a matching of the shock-cell and standing-wave wavenumbers, $k_s = k_{sw}$. This matching has been demonstrated across a wide range of operating conditions for round (Mercier *et al.* 2017), elliptical (Edgington-Mitchell, Honnery & Soria 2015) and twin (Knast *et al.* 2018) jets. However, the matching condition is only satisfied for some modes of jet screech; for a round jet the A1 mode is consistently observed to satisfy the matching condition, while the A2 mode does not. Due to the exactness of (1.3a,b), the mechanism governing some screech modes must either violate the assumptions underpinning (1.1), or the assumption of constant wave velocities is invalid. Testing with synthetic models suggests that inclusion of reasonable values of variation in convective velocity results in only minor differences in the peak wavenumber associated with the standing wave. Thus a significant discrepancy between the results of (1.1) and (1.3a,b) suggests that the former expression needs to be evaluated further. This paper will demonstrate how the two approaches can be reconciled, but further discussion of alternative methods of predicting screech is first warranted.

The expressions of Powell (1953) and Tam *et al.* (1986) generally perform very well in the A1 and B modes of jet screech; it is during the mode staging process that large discrepancies appear. There have, however, been some successful efforts to build predictive models that include mode staging. Gao & Li (2010) used numerical data to inform an empirical model for screech from circular jets across several modal stages. They noted that the number of concurrent waves (i.e. the sum of all extant downstream-propagating and upstream-propagating waves at a given instant in time) was lower for the A1 and B stages than for the A2 and C stages. On this basis they developed a prediction expression:

$$f_s = \frac{m}{nL}\frac{CD}{1 + M_c}. \tag{1.4}$$

Here m is the number of concurrent waves, n is the number of shock cells in the effective source region, L is the average shock cell spacing, C is a coefficient relating the convective Mach number to the ideally expanded jet velocity and D is the nozzle diameter. Their expression was able to accurately predict screech in the A1 and B modes using $m = 5$, and in the A2 and C modes using $m = 6$. The effective source region was held at $n = 5$ for both cases, on the basis of a subjective observation of apparent sources in the pressure fields of the numerical dataset. An extension of this approach can be found in the model of Mancinelli *et al.* (2021), which reduces the empiricism underpinning

the approach of Gao & Li (2010) by calculating wave properties via stability theory. This model achieves excellent agreement with experimental data for both the A1 and A2 modes with the variation of only one model parameter, which is once again the number of concurrent upstream- and downstream-propagating waves. Like in the work of Gao & Li (2010), an effective source location is used, but in this case at the fourth shock cell rather than the fifth. The success of these models suggests that the staging must be accompanied by a change in the relationship between the number of concurrent waves, and the effective region over which these concurrent waves are active in the resonance.

Central to the model of Mancinelli *et al.* (2021) is the idea that the upstream-propagating wave is not a free-stream acoustic wave, but a guided-jet mode (G-JM) first described in Tam & Hu (1989). That this G-JM could close the resonance loop in screech was first proposed in Shen & Tam (2002), who suggested that a switch between a free-stream acoustic wave and the G-JM could explain the A1–A2 mode staging. The presence of the G-JM in screeching jets has now been verified both numerically (Gojon, Bogey & Mihaescu 2018) and experimentally (Edgington-Mitchell *et al.* 2018), as well as numerically for ideally expanded (Bogey & Gojon 2017) and shock-containing (Gojon & Bogey 2017) impinging jets. Further, in a consideration of twin jets, which can exhibit a range of different coupling symmetries, it has been demonstrated that only those symmetries where the G-JM is propagative are observed in experimental data (Nogueira & Edgington-Mitchell 2021). Thus the suggestion of Shen & Tam (2002) that the G-JM might be a component of jet screech appears to have been prescient; however, they suggested that it might be active only in certain mode stages, while the present evidence suggests that the G-JM is actually the upstream component of all screech stages (Nogueira *et al.* 2022*b*). The G-JM only exists for a finite band of frequencies, and screech tones are observed to fall within this band, and be sharply cut off at its edges. Thus while Shen & Tam (2002) were correct regarding the importance of the G-JM, it does not appear to offer an explanation for the modal staging behaviour. There are several properties of the G-JM that set it apart from a free-stream acoustic wave. The first is the aforementioned cut-off behaviour; unlike acoustic waves, only certain frequencies of neutral G-JM are supported by a given flow. The second is the phase speed of the wave: the G-JM appears in the eigenspectra of both vortex-sheet and finite-thickness stability models as a discrete mode with a phase velocity slightly slower than the speed of sound, distinguishing it from the modes in the continuous acoustic branch. This difference in phase velocity is often very small, but is nonetheless a consistent characteristic of the G-JM. To return to the question of mode staging, without any evidence that a change in the nature of the upstream wave is responsible, a clear picture of mechanism is still lacking. While models such as that presented in Mancinelli *et al.* (2021) can accommodate modal staging, they do so by changing the concurrent number of waves in the resonance loop; why this might occur remains unclear.

Alongside the body of work supporting the G-JM as the upstream component of screech, another significant change in the present understanding of jet screech is the recent validation of a theory developed by Tam & Tanna (1982). Those authors suggested that triadic interactions between the Kelvin–Helmholtz (KH) wavepacket (with wavenumber k_{kh}) and the stationary shock structure (with wavenumber k_s) would transfer energy to other wavenumbers $k = k_{kh} \pm k_s$. This mechanism was demonstrated to be active in screeching jets for a range of conditions in Edgington-Mitchell *et al.* (2021*a*). In this recent work, it was also demonstrated that the fundamental result of Tam and Tanna could be reproduced through a linearization of the convective terms in the momentum equation, as

per (1.5) (note the sum and difference terms in the exponents on the second line):

$$\tilde{u}\partial_x\tilde{u} - U\partial_x U \approx ik_x U u' \exp(-i\omega t + ik_x x + im\theta)$$
$$+ iu' U_{sh}\tfrac{1}{2}\,(k_s \exp(-i\omega t + i(k_x + k_s)x + im\theta)$$
$$-k_s \exp(-i\omega t + i(k_x - k_s)x + im\theta))\,. \qquad (1.5)$$

The 'weakest-link' model in (1.1) results directly from the triadic interaction $k = k_{kh} \pm k_s$; it is an approximation to the absolute instability mechanism that has been demonstrated to underpin screech (Nogueira *et al.* 2022*b*). This would suggest that the theoretical underpinning of the weakest-link model is fundamentally correct (despite the original conception of the model involving free-stream acoustic waves rather than G-JMs). However, the model still provides no explanation for the mode staging behaviour consistently observed in screeching jets, and the frequency prediction based on this model as per (1.1) is fundamentally incompatible with the observation that $k_{sw} \neq k_s$ during some mode stages.

A reconciliation of the two equations and an explanation for mode staging behaviour in the context of Tam & Tanna (1982) was provided in the work of Nogueira *et al.* (2022*a*); in this work the A1–A2 staging was correctly predicted without the inclusion of any empiricism. At the core of this prediction was a consideration of the axial variation of the shock-cell structure, which in the spectral domain manifests as a series of suboptimal peaks $k_{s_{2:n}}$ in addition to the fundamental k_{s_1}. Note that this representation of the shocks via a Fourier transform in the axial direction is fundamentally different from the series representation in the original model of Tam & Tanna (1982), despite the similarities in nomenclature. In the original formulation, the wavenumbers in the series are restricted to those arising from the solution of the vortex-sheet dispersion relation at zero frequency, whereas in the present application they are just an empirical representation of the mean shock structure in the spectral domain; all wavenumbers are permitted. Critically, Nogueira *et al.* (2022*a*) demonstrated that the A1 mode of jet screech was associated with the KH wavepacket interacting with the fundamental peak, while the A2 mode was associated with an interaction with the first suboptimal. Both a local linear stability framework using experimental data and a consideration of absolute instability via the spatially periodic linear stability analysis framework produced robust predictions across the A1–A2 range of jet screech on this basis.

In this paper, we demonstrate the generality of the result of Nogueira *et al.* (2022*a*), showing that it not only provides an explanation for staging of the $m = 0$ modes in axisymmetric jet screech, but in fact accounts for all modal staging behaviour in screeching jets. Instead of an argument based on linear stability theory, here we provide evidence based on analysis of experimental data. With the role of suboptimal peaks in the shock-cell structure identified, the matching criterion $k_s = k_{sw}$ can be revisited; we demonstrate that the results of (1.1) and (1.3*a,b*) can be reconciled if the suboptimal peaks of the shock-cell structure $k_{s_{2:n}}$ are considered. The paper is organized as follows. In § 2 the two experimental datasets considered in this work are detailed, and the methods of analysis introduced. Spectral representations of the mean shock structure are compared with similar representations of the standing-wave pattern associated with resonance frequencies. Section 3 considers the different waves active in resonance: the KH wavepacket and the G-JM, and compares their wavenumbers with those predicted by the triadic-interaction model of Tam & Tanna (1982). The presence of multiple tones at a single operating condition is discussed in § 4. In § 5 the implications of the results presented in previous sections are discussed, along with a consideration of limitations in the analysis.

That section also includes a demonstration that the results can be extended to non-axisymmetric nozzle geometries, where the proposed mechanism performs similarly.

2. Shock structure and standing-wave patterns in screeching jets

2.1. *Experimental databases*

Two experimental databases are examined in this work, that of Li *et al.* (2021) (hereafter referred to as the Tsinghua data) as well as a previously unpublished dataset acquired at Monash University. Both datasets concern unheated jets operating at nozzle pressure ratios $NPR = p_o/p_\infty = [2.1 : 4]$, issuing from a purely converging nozzle of 10 mm diameter. For the Tsinghua data, the behaviour of the jets has already been classified: in this range the jet exhibits four stages of jet screech: A1 and A2, associated with $m = 0$ wavepackets, and B and C, associated with $m = 1$. Mode B manifests as a precessing flapping mode, and C as a purely helical oscillation. The Monash data are acquired for a jet of the same diameter over the same pressure ratio, but the nozzle geometry is quite different. The Tsinghua nozzle has a relatively large contraction from 25 to 10 mm, and a lip thickness of $0.5D$ (Li *et al.* 2021). The Monash nozzle is a single-jet equivalent of the geometry used in Bell *et al.* (2018); the nozzle has a lip thickness of only $0.15D$, and is relatively short with a smaller contraction. The largest difference in the facilities is the presence of a large solid plate approximately $2D$ upstream of the nozzle exit. The surface of this plate will both alter the entrainment field and produce a high reflection coefficient for upstream-propagating acoustic waves. The presence of reflective surfaces upstream has been shown to alter the staging behaviour of screeching (Norum 1983; Ponton & Seiner 1992) and impinging (Weightman *et al.* 2019) supersonic jets; the difference between the two nozzle geometries thus provides an additional means by which to interrogate staging mechanisms. For brevity, some exemplar data are provided from each dataset in the following sections, before both are used to demonstrate the main thesis of the paper. Though this paper is concerned principally with axisymmetric jets, which would suggest the use of a cylindrical coordinate system, the gradients measured by the schlieren technique are best described in Cartesian coordinates: x for the downstream direction, y for the transverse direction.

Both datasets contain images obtained via high-speed schlieren visualization, using Photon SA-Z cameras and pulsed LED illumination (Willert *et al.* 2010). For the data from Tsinghua, at each operating condition 2000 schlieren images of the $d\rho/dx$ gradient are obtained at a frame rate of 80 000 frames per second. The data are temporally averaged to produce mean fields $\bar{I}$, and dynamic mode decomposition (DMD) (Schmid 2010) is used to educe spatial modes ϕ at the resonance frequency. Further details of both the experimental set-up and the post-processing methodology are available in Li *et al.* (2021). For the Monash data, 50 000 images are obtained at a frame rate of 150 000 frames per second, and spectral proper orthogonal decomposition (SPOD) (Towne, Schmidt & Colonius 2018) is used instead to educe the spatial modes ϕ. The Monash schlieren data are supplemented by acoustic measurements performed using a GRAS Type 46BE 1/4″ pre-amplified microphone, positioned $10D$ downstream and $50D$ in the radial direction at an angle of $45°$ measured from the downstream axis (Stavropoulos *et al.* 2021). For each condition 500 000 samples were obtained at an acquisition frequency of 200 kHz, processed using the Welch method (Welch 1967) with 75 % overlap for windows of 4096 points. Figure 1 presents a comparison of the frequency spectra educed from both acoustic measurement and SPOD of schlieren data from the Monash facility. While some of the typical staging behaviour is evident, the presence of the upstream reflective surface results
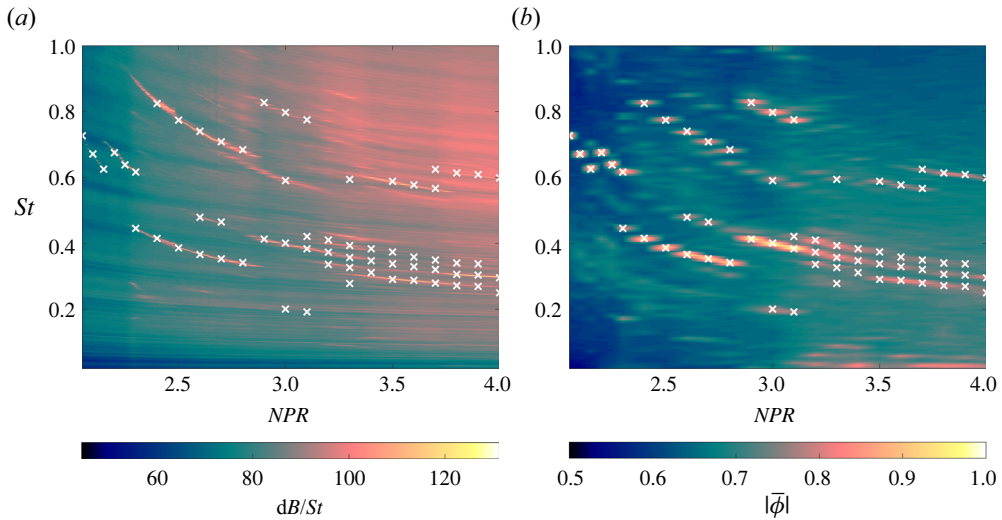
Figure 1. Frequency spectra as a function of nozzle pressure ratio for the Monash dataset from (*a*) acoustic measurements and (*b*) SPOD of schlieren measurements. The white crosses locate peaks identified in the SPOD spectra, and are overlayed on the acoustic data to demonstrate the close correspondence between the two methods of obtaining the spectra.

in the generation of many additional peaks not traditionally observed in screeching jets. As demonstrated in Li *et al.* (2021), the Tsinghua data follow a much more conventional mode staging trend.

This conventional trend is well exemplified in the DMD mode amplitudes (normalized such that $0 \leqslant |\phi| \leqslant 1$) spanning four mode stages of jet screech presented in figure 2. Periodic modulations are apparent in the shear layer and acoustic near field of each of the jets; these modulations are associated with the standing-wave structure of (1.3*a,b*). Li *et al.* (2021) observed several operating conditions where more than one mode was observed. Such multimodal behaviour is common in screeching jets, though whether the modes are simultaneous or mutually exclusive remains a topic of some debate (Mancinelli *et al.* 2019).

2.2. *Spectral representations of shock structure and standing waves*

From Nogueira *et al.* (2022*a*), a full consideration of the shock-cell structure is required to predict staging behaviour, and a spectral representation is an effective means to achieve this. In figure 3, time-averaged visualizations of the $\partial\rho/\partial x$ gradient from both datasets are presented, along with the absolute value of their accompanying streamwise Fourier transforms ($|\hat{\bar{I}}|$). The transform is performed along $y/D = 0$; while the relative amplitude of the second peak showed some sensitivity to the choice of radial position, the peak wavenumber was largely insensitive. The streamwise domain for the transform was $0 \leqslant x/D \leqslant 10$; by ten nozzle diameters downstream the intensity fluctuations associated with the shock cells were difficult to discern even at the highest nozzle pressure ratios. Note that while both datasets are measurements of the axial density gradient, the schlieren knife-edge is rotated by 180° between the two datasets, reversing the relationship between gradient and intensity. Despite the differences between the two facilities, the spectral representation of the shocks is consistently similar: a primary peak associated with the
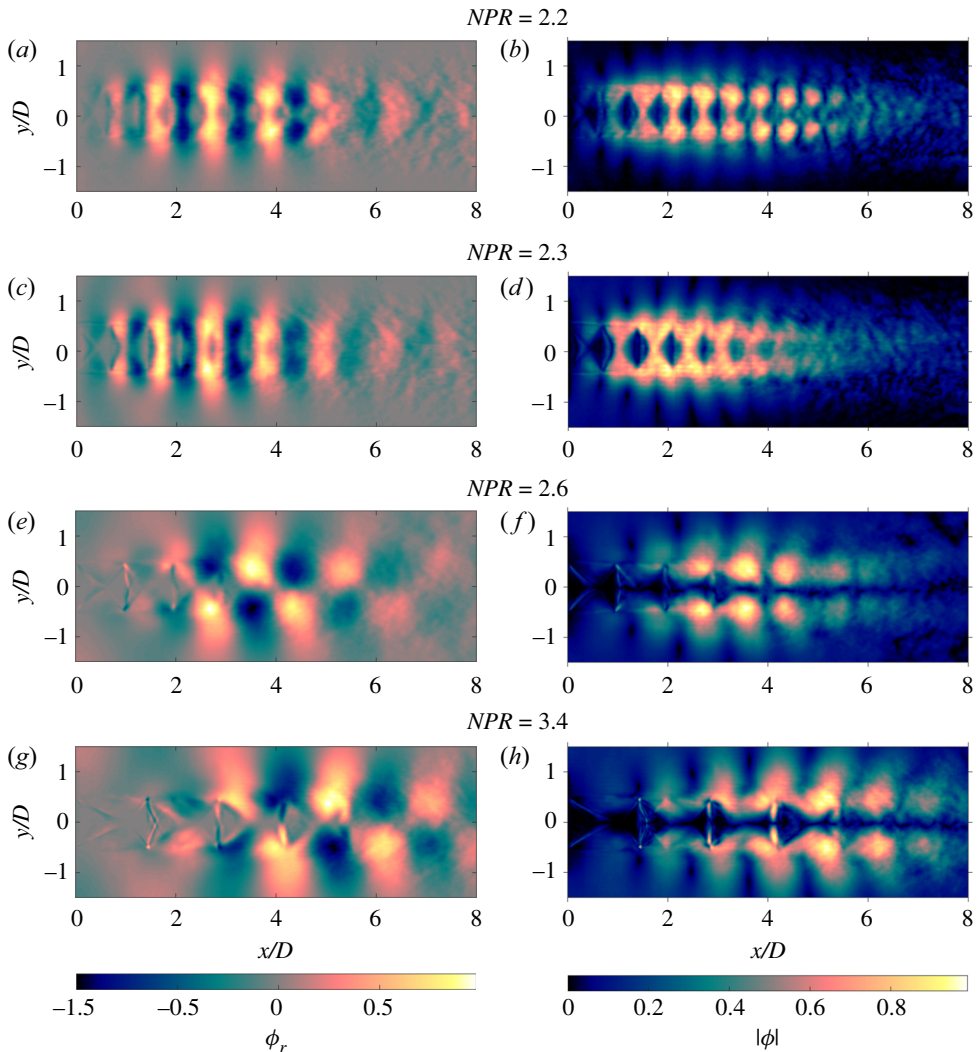
Figure 2. Exemplar DMD mode shapes as visualized by the real component (*a,c,e,g*) and corresponding amplitude fields (*b,d,f,h*) for the Tsinghua data. Represented here are the A1, A2, B and C modes of jet screech.

region where shock spacing is relatively constant, and a series of suboptimal peaks that represent the rapid variation in shock spacing that occurs further downstream.

Spectra for all operating conditions considered are presented as a contour in figure 4. Overlaid on this figure are white lines indicating transitions between screech mode stages. In both datasets, the first two lines are associated with the A1–A2 and A2–B transitions, respectively. In the Tsinghua dataset, there is an additional B–C transition at $NPR = 3.18$; the Monash data has a transition at $NPR = 2.9$, but as indicated in the spectra of figure 1 the region that follows the transition is complex and hard to classify. In both datasets the shock spectra exhibit not only the primary peak associated with the dominant shock wavenumber k_{s_1}, but also suboptimal peaks for all operating conditions, as well as harmonics of the first peak. Relative to other conditions, when the jet is in the flapping B mode the amplitude of the first suboptimal peak k_{s_2} is significantly weaker, but the
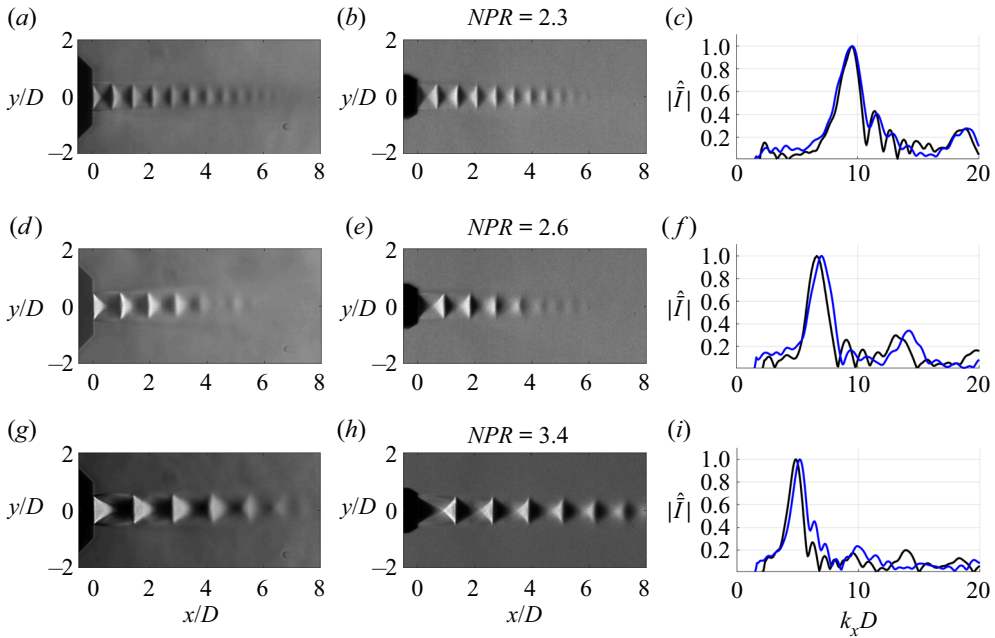
Figure 3. Time-averaged shock structures at three operating conditions for the Tsinghua (a,d,g) and Monash (b,e,h) data. (c,f,i) Results of axial Fourier transforms performed at the centreline of the images; Tsinghua wave spectra are in black, Monash are in blue.
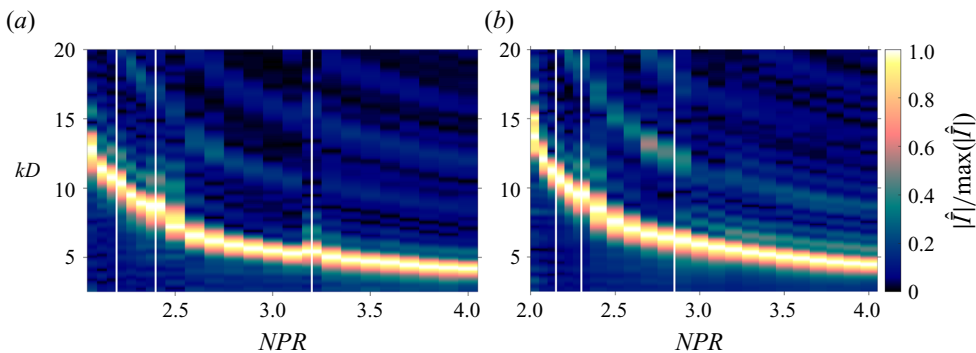

Figure 4. Axial wavenumber spectra of the mean shock structures in the flow. (a) Tsinghua data. (b) Monash data. Vertical white lines indicate pressures at which mode transitions occur.

harmonic of the first peak is stronger. To permit a comparison with k_{sw} in the analysis to follow, the wavenumbers k_{s_1} and k_{s_2} are extracted from the data presented in figure 4.

We now turn to a consideration of the standing waves evident in figure 2 to determine k_{sw}, and in doing so it is worth revisiting equation (1.2). The original expression presented in Panda (1999) assumed that the upstream-propagating wave had an acoustic phase velocity; the generalized expression we present does not. There is no question that screech generates high-amplitude free-stream acoustic waves; the tones associated with these waves are the original defining characteristic of screech. However, if the upstream-propagating wave that closes the screech feedback loop is not an acoustic wave, but the slightly subsonic G-JM, the expected wavelength of the standing wave would
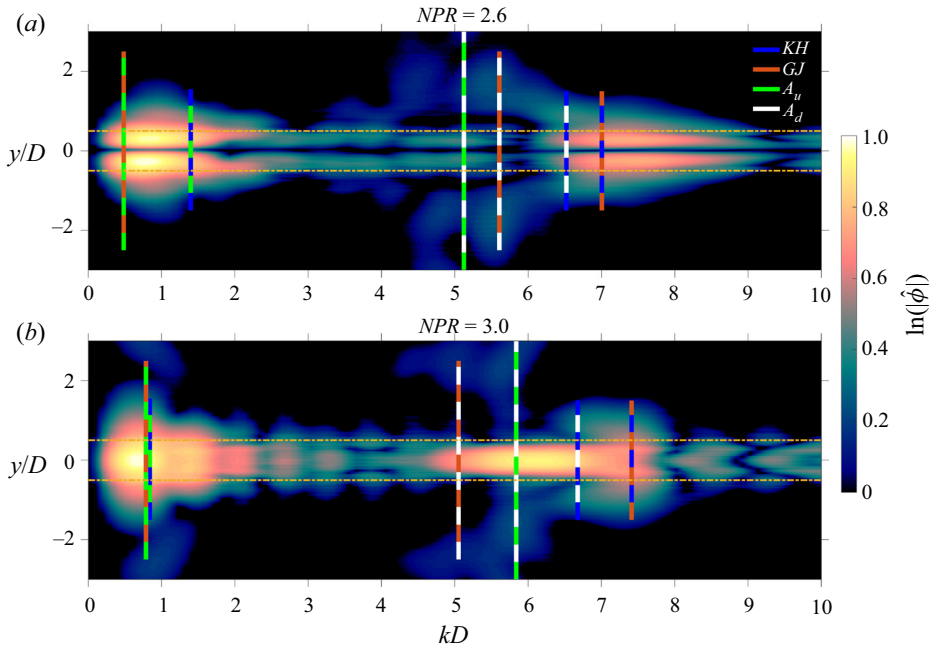
Figure 5. (*a*,*b*) Axial wavenumber spectra of standing wave structures (Monash data). Six predictions of standing waves are indicated by the vertical lines. Each line is made up of two colours, representing the two waves in the jet responsible for the standing wave in question. The dominant standing wave in the jet near field is expected to be that produced by the KH mode and G-JM, here indicated as the dashed blue and orange lines. Horizontal orange lines indicate the jet lipline at $y/D = \pm 0.5$.

be different in the shear layer of the jet and in the acoustic field. Close to the jet these may be difficult to discern, but the slower radial decay rate of the eigenfunctions associated with the acoustic wave (Tam & Hu 1989) suggests that at some distance outside the shear layer the free-stream acoustic waves should be significantly stronger than the G-JM. On this basis we would thus expect two standing waves of similar strength with slightly different wavenumbers in the near field of the jet. However, this is still an incomplete description. Outside the jet, there are signatures of the KH wavepacket, the G-JM, upstream-propagating acoustic waves associated with screech, but also downstream-propagating acoustic waves at the same frequency, either generated by shock–vortex interaction or directly by the KH wavepacket. There are thus not just one or two standing waves, but in fact a large number, of varying amplitude and wavenumber. This is exemplified in figure 5, which shows the spatial transform of the absolute value of the mode. Energy is distributed across a large range of wavenumbers. Overlaid on the image are lines indicating predicted standing waves based on interaction between the four aforementioned wave structures: the KH wavepacket, the G-JM, upstream-propagating acoustic waves and downstream-propagating acoustic waves. These predictions are based on an assumption that all the waves in question are represented by a single wavenumber. Nonetheless, the correspondence between the predictions and the wavenumber spectra is revealing. At low wavenumbers, there are standing waves associated with waves travelling in the same direction, which will not be discussed further. At higher wavenumbers, the interactions arise from waves travelling in opposite directions, and here there is a clear demonstration of the radial dependence of which standing waves will dominate. The wave resulting from the superposition of the KH wavepacket and G-JM is strongest at
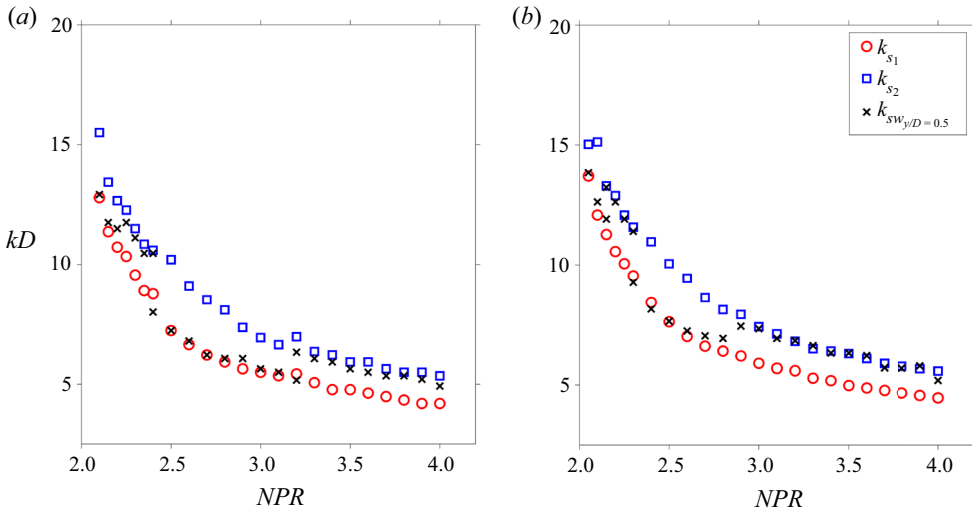
945 A8-10

Figure 6. Wavenumbers associated with the primary (k_{s_1}) and suboptimal (k_{s_2}) peaks of the shock-cell structure, and the standing waves associated with the G-JM (k_{sw_G}). (*a*) Tsinghua data. (*b*) Monash data.

the lipline of the jet, but rapidly decays in the radial direction. The superposition of the KH wavepacket and the upstream-propagating acoustic wave occurs at lower wavenumber, and while it is weaker at the lipline, it is slightly slower in its decay, meaning that at some distance from the jet, the dominant standing wave that would be extracted corresponds to this pair of waves instead. Further still from the jet is a standing wave formed between the upstream- and downstream-propagating acoustic waves. For the following analysis, a streamwise Fourier transform is taken of the absolute value of $|\phi|$ at $y/D = 0.5$, to capture the standing wave associated with the G-JM. The results for both datasets, along with the previously determined k_{s_1} and k_{s_2}, are plotted in figure 6.

There are several commonalities between the two datasets, but some key differences. The A1 mode is active for $NPR = [2.1 : 2.2]$ in both datasets; the A2 and B mode transitions occur at slightly lower NPR for the Monash data. The B mode is also significantly shorter in the Monash data, persisting only until $NPR \approx 2.8$ as opposed to $NPR \approx 3.2$ in the Tsinghua data. The helical C mode apparently persists until the end of the measurement range for both datasets; for brevity the designator 'C' will also be used to refer to the higher NPR modes, though as is discussed later, in the Monash data this mode is not actually an $m = 1$ helix traditionally associated with this mode stage. A close agreement of k_{sw} with k_{s_1} is evident for the A1 and B modes. More noteworthy is the close agreement between k_{sw} and k_{s_2} for the A2 and C modes. This is compelling evidence for the mechanism proposed in Nogueira *et al.* (2022*a*); the interaction of the KH wavepacket with suboptimal peaks in the shock wavenumber spectrum generates upstream-propagating waves that can close the resonance loop. These results are particularly striking at conditions characterized by switching between two modes of screech on rapid time scales (Li *et al.* 2021). In the Tsinghua data, excellent agreement is observed with k_{s_1} for the B mode at both $NPR = 2.4$ and $NPR = 3.18$, and with k_{s_2} for the A2 and C mode, respectively. Likewise in the Monash data, at $NPR = 2.3$, close agreement with k_{s_1} is observed for the B mode, and k_{s_2} for the A2 mode.

Finally, these results also offer a new perspective on the shock spectra presented in figure 4: the harmonic of the primary shock-cell peak is significantly stronger when
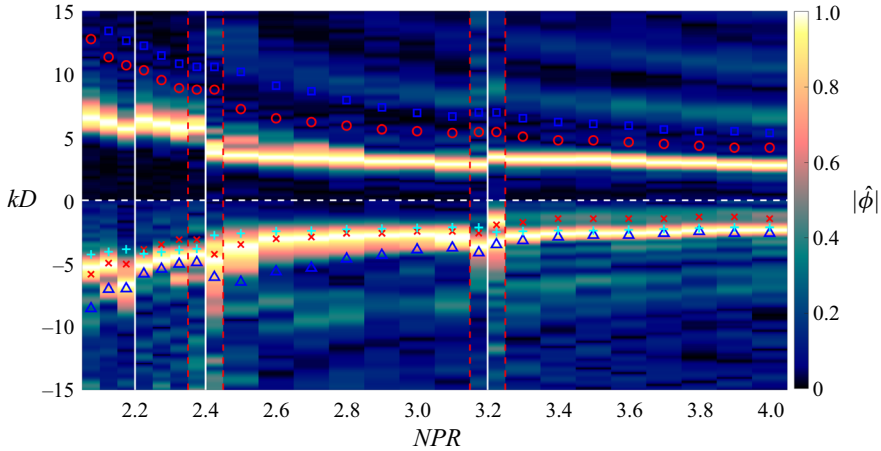
Figure 7. Tsinghua data axial wavenumber spectra $|\hat{\phi}|$. Spectra are normalized such that the peak amplitude for both positive and negative wavenumbers is $|\hat{\phi}| = 1$. Symbols: $\circ$, k_{s_1}; $\times$, $k_{kh} - k_{s_1}$; $\square$, k_{s_2}; $\triangle$, $k_{KH} - k_{s_2}$; $+$, k_a.

the jet is screeching in the flapping B mode. Conversely, the suboptimal peak k_{s_2} is significantly stronger at other conditions, and the wavenumber of this peak is very close to the wavenumber of the standing wave associated with the G-JM. This wavenumber matching suggests that there is a significant element of two-way coupling between the shock structures embedded in the jet and the resonance process; in a non-resonant jet there is no reason to expect a significant change in the shock structure with small changes in NPR, such as that observed between $NPR = 3.1$ and $NPR = 3.18$ in the Tsingua data, or $NPR = 2.8$ and $NPR = 2.9$ in the Monash data. The time-averaged structure of the shock cells is evidently governed not only by the pressure mismatch at the jet exit, but also by the standing wave associated with the resonance.

3. Waves active in different modes of jet screech

To further support the conjecture that the wavenumber of the G-JM is determined by interaction between the KH wavepacket and the various peaks of the shock cells, i.e. $k_{G-JM} = k_{kh} - k_{s_{1,2}}$, we now consider the waves active in the various stages of mode screech. Following the methodology presented in Edgington-Mitchell *et al.* (2021*a*), the spatial modes ϕ can be decomposed in the streamwise direction via a Fourier transform; the energy associated with each wavenumber is proportional to $|\widehat{\phi_k}|$. The results of this transform are presented as a function of NPR for the Tsinghua data (DMD modes) in figure 7 and for the Monash data (SPOD modes) in figure 8. The transform is performed across the entire axial domain at a radial position $y/D = 0.5$. Across the parameter space considered, there is consistent matching between the most energetic negative wavenumber (associated with the G-JM) and $k_{kh} - k_{s_1}$ for the A1 and B modes, and $k_{kh} - k_{s_2}$ for the A2 and C modes. The wavenumber associated with an acoustic wave of phase velocity $u_p = a_\infty$ sits consistently below the peak energy in the spectra, reinforcing that what is being measured is the G-JM rather than an acoustic wave. There are two notable exceptions to the aforementioned agreement with the expected wavenumber associated with a given mode and the peak energy. These exceptions occur at pressures associated with mode transitions, and are clearest in the Tsinghua data at $NPR = 2.2$ and $NPR = 3.18$. These transitions involve a switch from the resonance being closed via the interaction of the KH
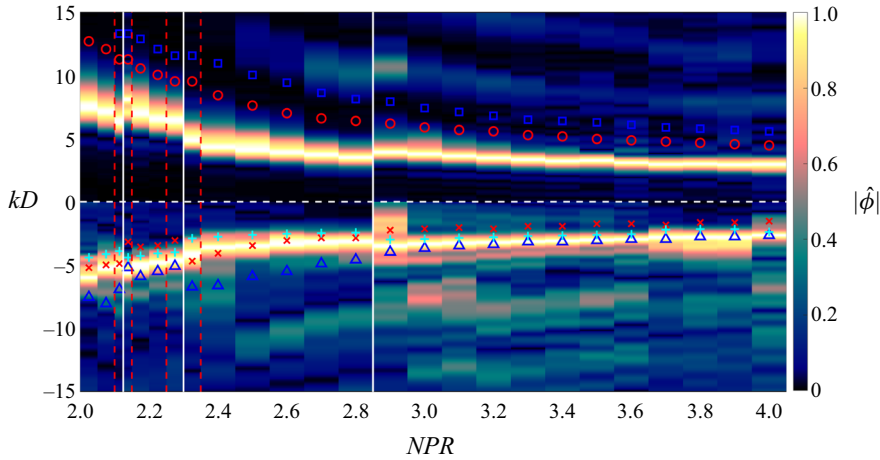
945 A8-12

Figure 8. Monash data axial wavenumber spectra $|\hat{\phi}|$. Spectra are normalized such that the peak amplitude for both positive and negative wavenumbers is $|\hat{\phi}| = 1$. Symbols: $\circ$, k_{s_1}; $\times$, $k_{kh} - k_{s_1}$; $\square$, k_{s_2}; $\triangle$, $k_{KH} - k_{s_2}$; $+$, k_a.

wavepacket and the primary shock-cell peak k_{s_1} to the suboptimal peak k_{s_2}. The data here suggest that even before the mode switch occurs, there is significant energy associated with the interaction of the KH wave and the suboptimal peak. This is evident even at $NPR = 2.15$ in the Tsinghua data; while the dominant peak is at $k_{kh} - k_{s_1}$ there is a peak at $k_{kh} - k_{s_2}$. By $NPR = 2.2$ this secondary peak has grown stronger than the primary, a harbinger of the mode switch that occurs at $NPR = 2.25$. A strengthening of a peak at $k_{kh} - k_{s_2}$ is also evident in the Monash data at $NPR = 2.8$, prior to a mode switch, but this peak is still significantly weaker than the primary $k_{kh} - k_{s_1}$ peak.

A clearer demarcation between upstream-propagating acoustic waves and the G-JM can be observed when considering the radial structure of the streamwise wavenumber spectra. Four such exemplar spectra, chosen to represent each of the screech modes active in these facilities, are provided for the Tsinghua (figure 9) and Monash (figure 10) data. At $NPR = 2.15$ the jet is still screeching in the A1 mode, but from figures 7 and 8 at $y/D = \pm 0.5$ there is significant energy associated with the $k_{kh} - k_{s_2}$ interaction. When considered as a function of radius, this becomes clearer; while there are peaks in the shear layer associated with interactions between the KH wavepacket and both k_{s_1} and k_{s_2}, the former has significant support outside the shear layer, while the latter rapidly decays. This suggests that while triadic interactions between the KH wavepacket and the shock cells are distributing energy to both wavenumbers, the response of the flow to this distribution of energy is different. The resultant wave at $k_{kh} - k_{s_1}$ is the G-JM while at $k_{kh} - k_{s_2}$ the mode appears to be duct-like. Stability theory predicts a duct-like mode with positive group but negative phase velocity that can appear at these wavenumbers (Towne *et al.* 2017); it may be that this duct-like mode is being energized by the interaction between the KH and the shock suboptimal, but with positive group velocity this wave is unable to close the resonance. At $NPR = 2.3$, the energy associated with $k_{kh} - k_{s_2}$ is no longer bounded within the jet; this is now the signature of a G-JM capable of supporting resonance. This is significantly easier to see in the Tsinghua data; in the Monash data, $NPR = 2.3$ is perhaps the case with the least clear agreement in the entire dataset. Nonetheless in both sets of data it is clear that there is little energy at $k_{kh} - k_{s_1}$ in the A2 mode. The B mode at $NPR = 2.8$ (Monash) or 2.9 (Tsinghua) shows significant energy at $k_{kh} - k_{s_1}$, extending well outside the shear layer. Consistent across all cases considered here, irrespective of whether the
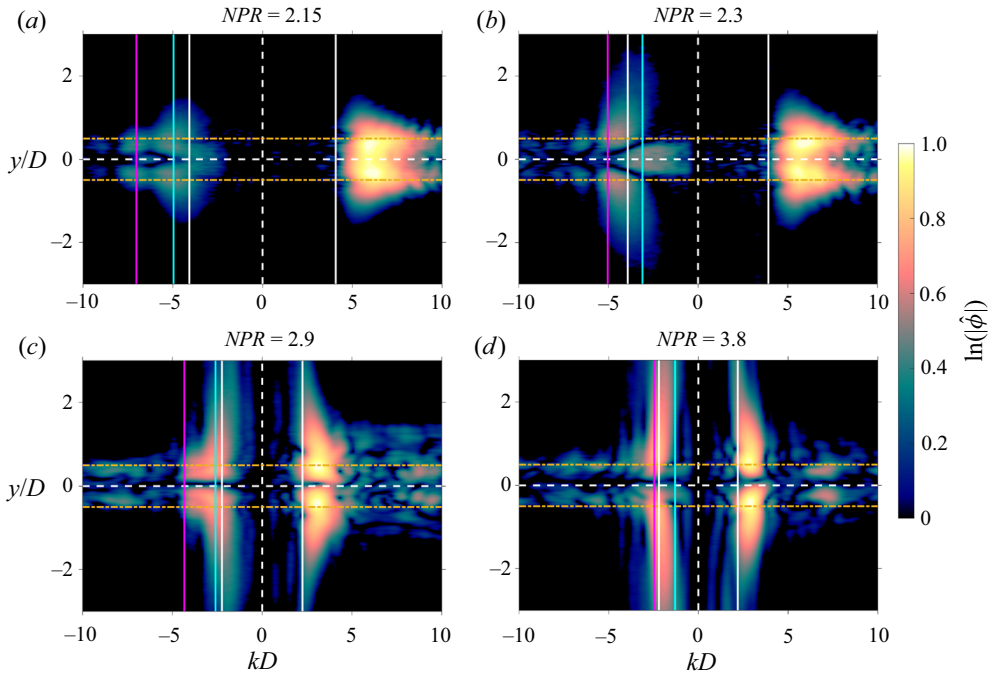
Figure 9. Tsinghua data wavenumber spectra as a function of radial position. Cyan vertical line, $k_{kh} - k_{s_1}$; magenta vertical line, $k_{kh} - k_{s_2}$; white vertical line (solid), $\pm k_a$; white lines (dashed), zero axis; orange horizontal lines, $y/D = \pm 0.5$.

peak energy in the shear layer occurs at $k_{kh} - k_{s_1}$ or $k_{kh} - k_{s_2}$, is that by $|y/D| > 2$ the peak energy shifts to k_a. This is a significant result, as it suggests that while a triadic interaction between the KH wavepacket and the shock structures energizes the G-JM, it does not directly generate the upstream-propagating sound waves associated with screech. Instead, the energy leaked to supersonic wavenumbers in the spectral domain permits the generation of high-amplitude acoustic waves directly upstream via a mechanism similar to that of Mach-wave radiation, as originally suggested in Tam & Tanna (1982).

4. Multimodal jet screech

Multiple frequency peaks at a single operating condition are evident in both datasets, suggesting that more than one screech loop is active at these conditions. The coexistence of multiple tones at $NPR = 2.3$ in the Monash data has already been mentioned. Figure 11 presents SPOD modes with accompanying axial wavenumber spectra for both tones evident at this condition. The higher-frequency tone is evidently associated with an $m = 0$ axisymmetric mode (the A2 mode of jet screech), while the lower-frequency tone is an $m = 1$ mode, likely a flapping B mode (though demarcation between flapping and purely helical modes cannot be rigorously determined from schlieren). The wavenumber spectra demonstrate once again the closure of the A2 mode via $k_{kh} - k_{s_2}$ and the B mode via $k_{kh} - k_{s_1}$. Multimodality appears at a slightly higher pressure of $NPR = 2.4$ in the Tsinghua data, but is otherwise qualitatively the same as what is evident in figure 11. At $NPR = 3.18$, the Tsinghua data exhibit a simultaneous B and C mode (both $m = 1$ modes), which is consistent with the typical staging behaviour of screeching axisymmetric jets. The Monash jet, issuing from a nozzle with a large flange slightly upstream of the nozzle
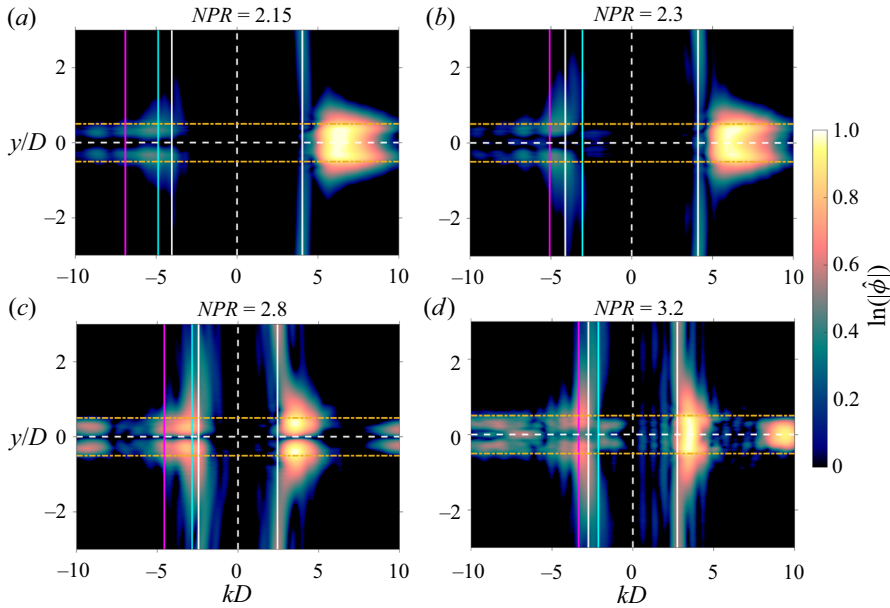
945 A8-14

Figure 10. Monash data wavenumber spectra as a function of radial position. Cyan vertical line, $k_{kh} - k_{s_1}$; magenta vertical line, $k_{kh} - k_{s_2}$; white vertical line (solid), $\pm k_a$; white lines (dashed), zero axis; orange horizontal lines, $y/D = \pm 0.5$.

Figure 11. Two screech modes at $NPR = 2.3$ (Monash data): (a,b) $St = 0.62$; (c,d) $St = 0.45$. Cyan vertical line, $k_{kh} - k_{s_1}$; magenta vertical line, $k_{kh} - k_{s_2}$; white vertical line (solid), $\pm k_a$; white lines (dashed), zero axis; orange horizontal lines, $y/D = \pm 0.5$.
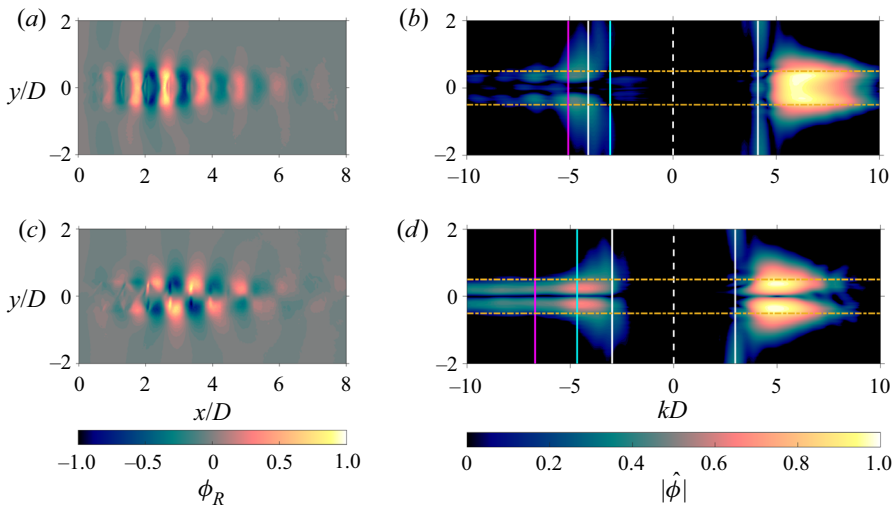
exit, presents significantly different multimodal behaviour for $NPR \geqslant 2.9$. As per figure 1, there are conditions whose SPOD modes exhibit up to four spectral peaks in a relatively narrow band of frequency, none of them being harmonics of the other. Some of these modes clearly correspond to peaks in the acoustic spectra, for others the correlation is less clear.
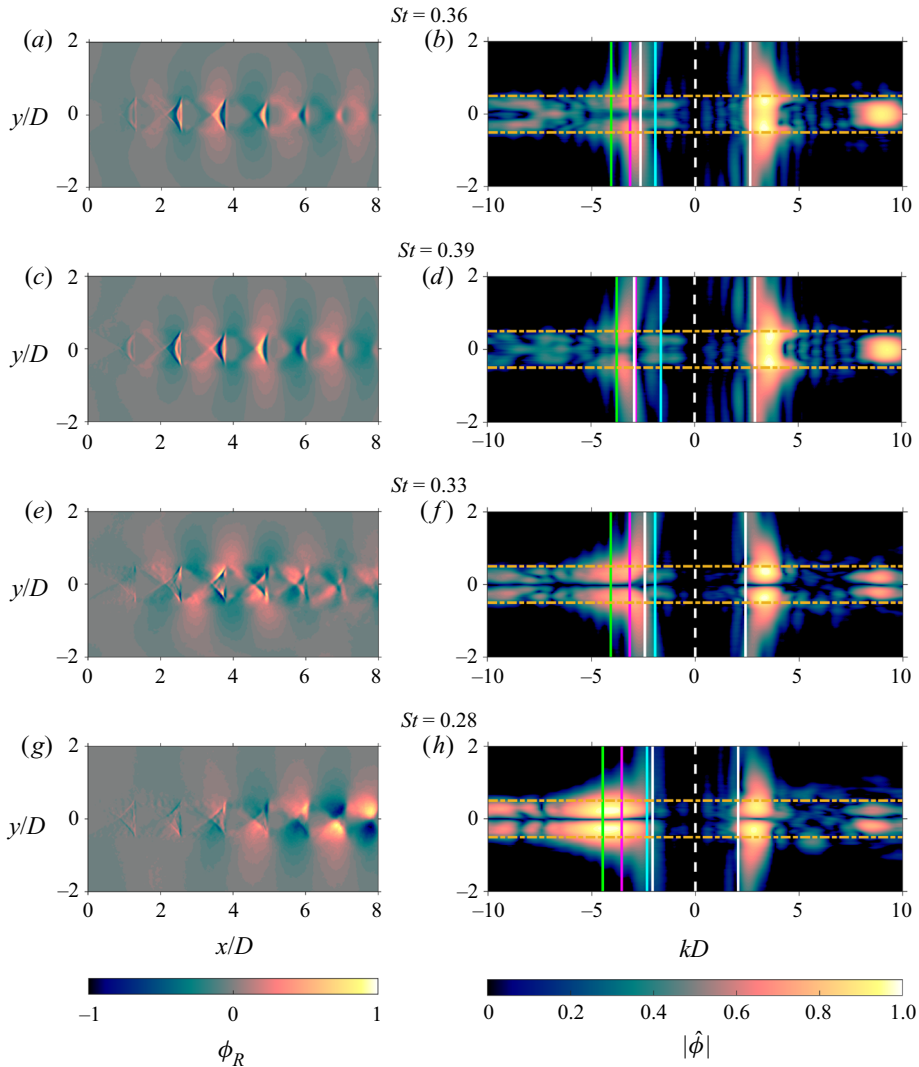
Figure 12. Four screech modes at $NPR = 3.3$ (Monash data): (a,b) $St = 0.36$; (c,d) $St = 0.39$; (e,f) $St = 0.33$; (g,h) $St = 0.28$. Cyan vertical line, $k_{kh} - k_{s_1}$; magenta vertical line, $k_{kh} - k_{s_2}$; green vertical line, $k_{kh} - k_{s_3}$; white vertical line (solid), $\pm k_a$; white lines (dashed), zero axis; orange horizontal lines, $y/D = \pm 0.5$.

Figure 12 presents modes and associated wavenumber spectra for the four spectral peaks in the range $0.25 \leqslant St \leqslant 0.4$. The modes are presented here in order of SPOD modal energy, though noting that in performing SPOD on schlieren images, the energy relates to intensity fluctuations rather than directly to any fluid variable. The most energetic mode at this condition is an $m = 0$ mode, whose G-JM is energized by the $k_{kh} - k_{s_2}$ interaction. This in itself may be somewhat surprising, as the classical view of jet screech is that $m = 0$ modes are only evident in the A1 and A2 modes at relatively low levels of underexpansion. However, Li *et al.* (2021) did provide evidence of a weak $m = 0$ mode at pressures typically assumed to be dominated by $m = 1$ modes. Here, likely as a result of the unusual boundary conditions of the experimental facility, we find an $m = 0$ mode to be dominant, at least through the lens of the schlieren technique. Skipping ahead for a moment, the third-most

energetic mode is an $m = 1$ mode, also closed by the $k_{kh} - k_{s_2}$ interaction. The multimodal behaviour observed at lower pressure ratios was always accompanied by a switch between the G-JM being driven by either $k_{kh} - k_{s_1}$ or $k_{kh} - k_{s_2}$; this result shows that multimodality can also be underpinned by the same triadic interaction, but with different azimuthal wavenumbers. It is the second- and fourth-most energetic modes, however, that are perhaps the least expected; in these cases we find that the G-JM appears to be energized by $k_{kh} - k_{s_3}$, which is a triadic interaction between the KH wavepacket and the third peak of the axial shock spectrum. This once again manifests for both $m = 0$ and $m = 1$ azimuthal modes. Despite the presence of four distinct peaks, none are observed that involve the classical $k_{kh} - k_{s_1}$ interaction. The SPOD modes associated with the $k_{kh} - k_{s_3}$ interaction are almost as 'energetic' as those associated with $k_{kh} - k_{s_2}$.

5. Discussion

5.1. *Interpretation of the wavenumber spectra*

The idea that different stages of jet screech might involve shocks at different distances downstream of the jet is not new, as but one example (Mercier *et al.* 2017) showed that the effective source position shifted between different modes of jet screech. The result here, however, is underpinned by a fundamentally different concept. Nogueira *et al.* (2022*b*) demonstrated that screech could be predicted simply through a consideration of mean-flow periodicity, without a requirement that this periodicity arose from shock cells. The present analysis supports the requirement of periodicity (implicit in the use of wavenumber to characterize the flow), but the interpretation of suboptimal peaks in the axial wavenumber spectrum is not necessarily an intuitive one. These peaks evidently represent a variation in the wavelength of the periodicity, but to which part of the jet they correspond in the spatial domain is less clear. Shock spacing is continuously varying, and thus it is not straightforward to associate the suboptimal peaks with given regions of the jet. Here we attempt to elucidate the significance of these suboptimal peaks. To link the spectral results to the spatial domain, we perform a series of axial wavenumber transforms on a smaller window, which is translated through the larger domain in the manner of a spectrogram, permitting a localization in space. The window size is set to π/k_{s_1}, i.e. a length of two shock cells. For each condition, the local window that best matches each of k_{s_1}, k_{s_2} and k_{sw} is identified. A comparison of the results from the use of these local windows is indicated in figure 13 as k'. Across all pressure ratios considered, it is clear that the primary peak k_{s_1} can be well represented by two shock cells, i.e. $k'_{s_1} = k_{s_1}$. While for many cases this local window was located across the first two shock cells, this was not true for all cases. For most cases considered, the secondary peak in the full transform can be shown to correspond to a local quasi-periodicity somewhere in the flow, $k'_{s_2} \approx k_{s_2}$. The location of the window to produce this match ranged from starting at the fifth shock cell to the eighth. These results suggest that the most straightforward interpretation of the peaks in the original shock spectra is that they do capture the local quasi-periodicity somewhere in the flow, though the exact position it corresponds to depends on the individual spectrum. To further support this point, we also select the window whose primary wavenumber corresponds to k_{sw}; here we denote this k'_{sw}. We see very close agreement across almost the entire range of conditions, except at the highest pressure ratios, where the shock train continues well past the end of the imaging domain, and the local approach is thus constrained. The agreement is at some conditions better than that originally demonstrated in figure 6. On this basis, it can be stated that the relation $k_G = k_{KH} - k_s$ can be satisfied by a local quasi-periodicity of wavenumber k_{s_L}, which can occur at a range of different axial positions.
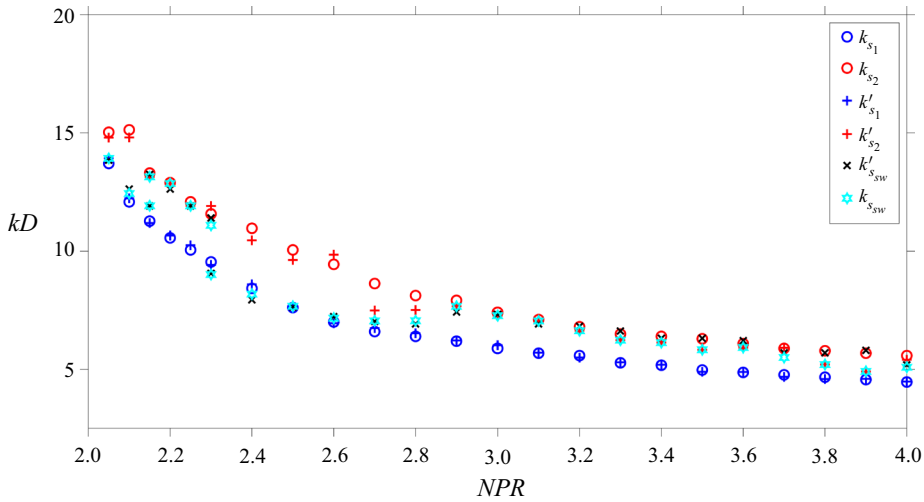
Figure 13. Comparison of local and 'global' axial transforms of the shock structure on Monash data. Here k indicates wavenumbers calculated from a transform on the entire domain and k' indicates wavenumbers calculated by choosing maximum agreement from a sliding short-window fast Fourier transform.

5.2. *Mode staging in non-axisymmetric jets*

All the evidence presented for this mechanism thus far has been for axisymmetric jets; however, modal staging is exhibited by a range of nozzle geometries including elliptical and rectangular (Zaman 1995). To demonstrate that the staging behaviour can be accurately described by a switch from the G-JM being associated with wavenumbers $k_{kh} - k_{s_1}$ to $k_{kh} - k_{s_2}$, we consider the elliptical jet data presented in Edgington-Mitchell *et al.* (2015). In those data, the elliptical jet is observed to undergo five distinct stages in the range $2 \leqslant NPR \leqslant 5$. Here we consider two cases that occur at similar pressure ratios to the 'B' and 'C' modes observed in the axisymmetric jet (though noting that this is not a helical mode in the Monash data). The wavenumber spectra presented in figure 14 suggest that despite the very different azimuthal structure of elliptical jets, the mode staging transition is still governed by triadic interaction between the KH wavepacket and various peaks in the streamwise shock spectra. At $NPR = 2.6$, which sits in a region of smooth frequency variation equivalent to the B mode in the Tsinghua axisymmetric-jet data, the G-JM is located at $k_{kh} - k_{s_1}$ for the elliptical jet, just as it is for the axisymmetric jet. At $NPR = 3.2$, the elliptical jet has jumped to a higher frequency, similar to the B–C mode staging in an axisymmetric jet; for this higher frequency, the G-JM sits close to $k_{kh} - k_{s_2}$, once again just as it does in the axisymmetric jet. Particularly noteworthy is that in the elliptical jet this is not associated with a change in dominant azimuthal mode; modal staging behaviour other than the A1–A2 transition has most often been associated with changes in the symmetry (azimuthal or otherwise) of the dominant screech mode. The present results indicate that this is not necessarily the case.

While many non-circular nozzles do exhibit screech, there are typically fewer stages; Zaman (1995) and Panda *et al.* (1997) noted a single-stage transition for aspect ratio $AR = 3$ rectangular and elliptical nozzles. Rectangular (Raman & Rice 1994; Lin & Powell 1997; Alkislar, Krothapalli & Lourenco 2003) and elliptical (Rao, Kushari & Chandra Mandal 2020) jets with $AR \geqslant 4$ have not been observed to exhibit staging behaviour at all. The present results suggest that the secondary (or tertiary) peak in the shock-cell
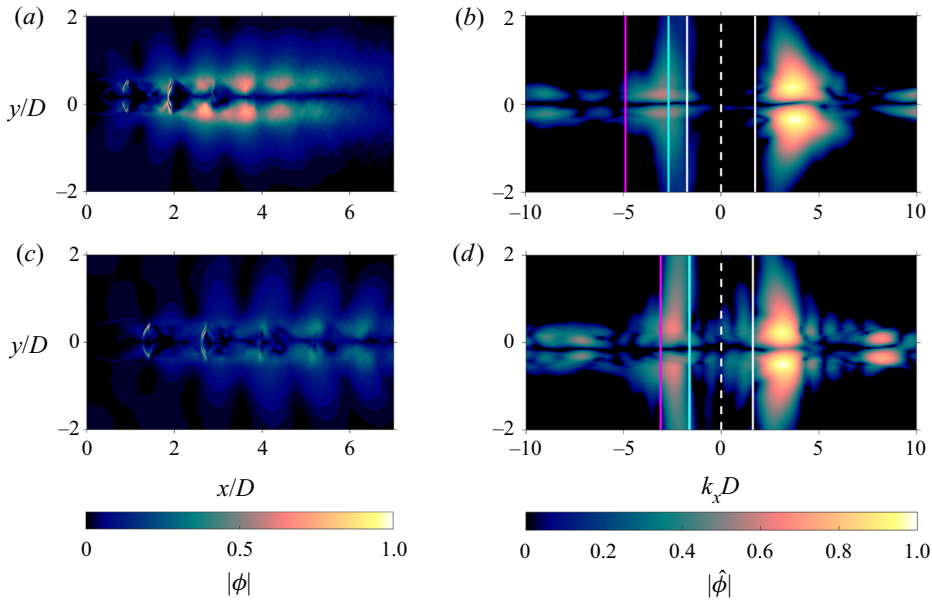
945 A8-18

Figure 14. Wavenumber spectra for an $AR = 2$ elliptical jet operating at two different modal staging conditions: (*a*,*b*) $NPR = 2.6$; (*c*,*d*) $NPR = 3.2$ (Edgington-Mitchell *et al.* 2015). (*a*,*c*) The absolute value of the complex POD mode pair ϕ. (*b*,*d*) The axial wavenumber spectrum corresponding to these modes. Cyan vertical line, $k_{kh} - k_{s_1}$; magenta vertical line, $k_{kh} - k_{s_2}$; white vertical line (solid), $\pm k_a$; white lines (dashed), zero axis.

spectrum may be a necessary component of the mode transitions in jet screech, which now provides an explanation for why staging is not observed for jets at these higher ARs. As the AR of elliptical or rectangular jets is increased, the strength of the flapping mode associated with screech also increases, resulting in a more rapid breakdown of the shock structures in the jet. When this decay of the shock cells is sufficiently rapid, there is no distinct suboptimal peak in the shock wavenumber spectrum, and thus no mechanism for a mode switch to occur. Figure 15(*a*) presents wavenumber spectra for screeching rectangular jets with $AR = [2, 4]$; while a strong secondary peak is visible for the $AR = 2$ jet, there is only a single broad peak with no clear suboptimals at $AR = 4$ (though one may well be hidden beneath the broad primary peak). Schlieren images of the mean shock structures are provided in figure 15(*b*), where the more rapid decay at $AR = 4$ is visible. The instantaneous colour schlieren image presented in figure 15(*c*) shows the vortices of the KH wavepacket on a significantly larger scale than the jet itself, and the shocks being displaced radially by as much as half a jet width by the third shock cell. It is worth emphasizing, however, that there need not be a sharp peak in the shock spectra to underpin resonance; all wavenumbers will transfer energy to other wavenumbers via triadic interaction with the KH wavepacket. This transfer is a necessary, but insufficient component of jet screech; there must be a neutral or weakly damped G-JM at this wavenumber and frequency to then transport this energy back upstream (Gojon *et al.* 2018; Gojon, Gutmark & Mihaescu 2019; Mancinelli *et al.* 2021), and in turn a sufficiently unstable KH wavepacket, etc. In essence, these triadic interactions simply form one necessary component of the overall global stability of the system (Nogueira *et al.* 2022*b*).
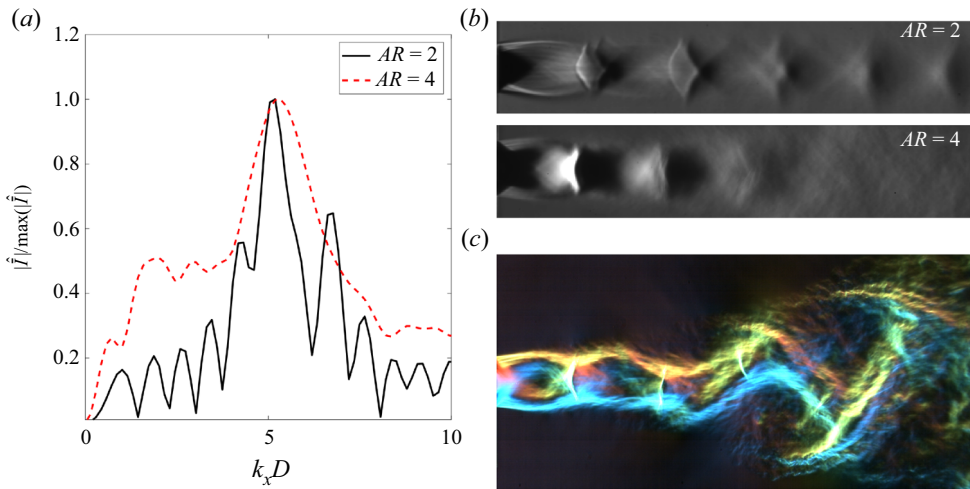
Figure 15. (*a*) Spatial wavenumber spectra of mean shock structure for rectangular jets at $AR = [2, 4]$. (*b*) Temporally averaged schlieren images used to produce these spectra. (*c*) Instantaneous colour schlieren image demonstrating breakdown of shock-cell structure for $AR = 4$ jet.

5.3. *The mechanism of far-field sound generation*

Amongst the most persistent debates on the topic of jet screech is the question of whether screech tones are produced at a single source, or by a distribution of sources. There is some compelling evidence on both sides. The present results demonstrate that the directivity of screech can be explained purely in the context of a distributed source, as originally proposed by Tam *et al.* (1986). This can be shown explicitly via a consideration of the wavenumber spectra presented earlier in figures 9 and 10. In these data, energy is distributed across a range of acoustically matched wavenumbers, i.e. spanning the range $k = [-k_a, k_a]$. The expected acoustic radiation pattern that results from this wavenumber distribution can be obtained using the wavy-wall analogy of Tam & Tanna (1982), though with the heavy caveat that these wavenumbers are derived from a decomposition of schlieren images; the energy associated with a particular wavenumber in these measurements does not correspond directly to any property responsible for sound radiation. Nonetheless, exemplar wavenumber spectra and the accompanying radiation patterns are presented in figure 16.

Despite the highly qualitative nature of the data, the relative strength of the upstream and downstream directivity is consistent with that measured in Norum (1983). This provides empirical confirmation that the upstream directivity of screech can be explained directly by the Mach-wave radiation mechanism of Tam *et al.* (1986). Given that such a wavenumber distribution can arise without the need for shocks in the flow at all (only the periodicity that results from them, as per Nogueira *et al.* (2022*b*)), this would seem to suggest that the shocks themselves might play little role beyond their role in transferring energy via triadic interaction. Measured against this, however, are a number of experimental studies which either suggest the far-field sound arises at a single source, or directly visualize sharp shock-like acoustic wavefronts emanating from the shocks in the flow. As examples of the former, both Raman (1997) and Mercier *et al.* (2017) localize the screech source to a single shock cell, for rectangular and axisymmetric jets, respectively. However, in both cases the localization was based on an *a priori* assumption that screech did indeed arise at a single 'effective' source, which as Raman (1997) notes is not incompatible with
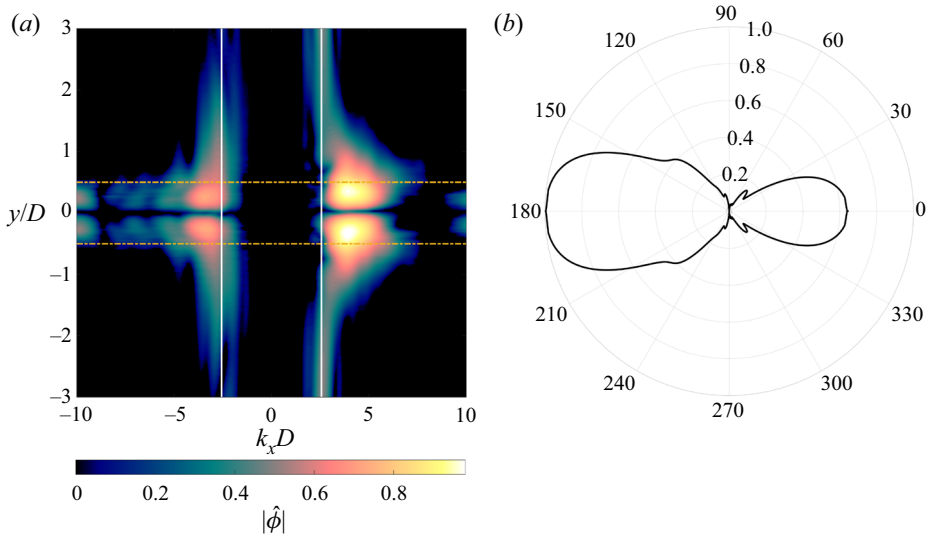
Figure 16. Wavenumber spectra (*a*) and acoustic directivity from acoustically matched wavenumbers (*b*) for $NPR = 2.6$ (Monash data).

distributed sources. Using schlieren images rather than acoustic measurements, Semlitsch *et al.* (2020) identified a single effective source in a rectangular jet, located near the third and fourth shock cell. The evidence on this basis for a single source is thus inconclusive; in contrast, the evidence for the direct visualization of sound waves emitted from shocks is extensive. Poldervaart, Vink & Wijnands (1968) is likely the first visualization of a screeching jet showing sharp, shock-like waveforms apparently emitted from shocks within a planar screeching jet. Close inspection of the video reveals the 'shock leakage' process is well captured, and far-field acoustic waves unambiguously arise from this process. Further, Poldervaart *et al.* (1968) demonstrated that the reflection of these waves from upstream reflectors could enhance or suppress the entire resonance loop, suggesting they were responsible not only for far-field sound, but also for the upstream-propagating component of the feedback loop. Schlieren visualizations in Raman (1997), Alkislar *et al.* (2003) and Semlitsch *et al.* (2020) also show sharp, high-amplitude waveforms arising from a shock in a rectangular jet, as do the high-fidelity simulations of Berland, Bogey & Bailly (2007). A theoretical basis for this process was provided in the works of Manning & Lele (2000), Suzuki & Lele (2003) and Shariff & Manning (2013), and experimental evidence of the process was provided for rectangular jets in Semlitsch *et al.* (2020), and both single and twin axisymmetric jets in Edgington-Mitchell *et al.* (2021*b*).

How then to reconcile the success of linear models based only on the wave-like nature of the flow (Nogueira *et al.* 2022*b*) with these clear observations of highly nonlinear processes such as shock leakage producing high-amplitude tones? In this paper we have provided evidence that screech mode selection is underpinned by triadic interactions between the KH wavepacket and local quasi-periodicity in the shock structures. These triadic interactions also transfer energy to a range of acoustically matched wavenumbers that can provide a reasonable explanation of the directivity pattern of a screeching jet. What is not available from this model, however, is any prediction of amplitude for this acoustic radiation. The evidence suggests that both linear (radiation from acoustically matched wavenumbers) and nonlinear (shock leakage) mechanisms contribute to the radiated sound. For axisymmetric jets and low-AR non-axisymmetric jets, the triadic

interaction mechanism controls the frequency selection, and shock leakage appears to be simply a correlated process not directly involved in the feedback loop. In high-AR jets, such as those studied in Poldervaart *et al.* (1968), it may well be that the sound produced by the shock leakage is indeed responsible for closing the feedback loop. Further work is needed to determine the relative contributions of the two mechanisms.

6. Conclusions

A clear explanation of the mechanism underpinning mode staging in jet screech has eluded researchers since Powell first identified the phenomenon. In explaining this mechanism, we believe we have provided a general theory that describes jet screech:

> In a screeching jet, triadic interactions occur between the KH wavepacket and regions of local quasi-periodicity in the flow associated with the shock structure, represented by peaks in the streamwise wavenumber spectrum. These interactions energize a range of wavenumbers, including the G-JM, which propagates upstream to close the resonance loop. Nonlinear interactions between the wavepacket and the shocks also produce high-amplitude acoustic radiation that contributes to the far-field sound, but in axisymmetric jets this acoustic radiation is not directly involved in the resonance process.

Alongside this core theory, the paper has also demonstrated that close to modal transition points, energy is transferred by interaction with both the primary and suboptimal peaks, with the amplitude of the latter increasing as transition points are approached. Multiple standing waves exist in the near field of screeching jets, between downstream-propagating KH wavepackets, upstream-propagating G-JMs and acoustic waves propagating in both directions. The mode staging mechanism presented here is not limited to axisymmetric geometries; low-AR non-axisymmetric jets should be expected to exhibit similar behaviour associated with these suboptimal peaks. Finally, the mechanism also explains the absence of staging behaviour for high-AR elliptical and rectangular jets; the rapid decay of the shock structure precludes the existence of a suboptimal peak in the shock spectrum.

Declaration of interests. The authors report no conflict of interest.

Author ORCIDs.

Daniel Edgington-Mitchell https://orcid.org/0000-0001-9032-492X;

Xiangru Li https://orcid.org/0000-0002-7817-2975;

Nianhua Liu https://orcid.org/0000-0002-5652-2196;

Petronio Nogueira https://orcid.org/0000-0001-7831-8121.

REFERENCES

ALKISLAR, M., KROTHAPALLI, A. & LOURENCO, L. 2003 Structure of a screeching rectangular jet: a stereoscopic particle image velocimetry study. *J. Fluid Mech.* **489**, 121–154.

BELL, G., SORIA, J., HONNERY, D. & EDGINGTON-MITCHELL, D. 2018 An experimental investigation of coupled underexpanded supersonic twin-jets. *Exp. Fluids* **59** (9), 139.

BERLAND, J., BOGEY, C. & BAILLY, C. 2007 Numerical study of screech generation in a planar supersonic jet. *Phys. Fluids* **19** (7), 075105.

BOGEY, C. & GOJON, R. 2017 Feedback loop and upwind-propagating waves in ideally expanded supersonic impinging round jets. *J. Fluid Mech.* **823**, 562–591.

CLEM, M.M., ZAMAN, K.B.M.Q. & FAGAN, A.F. 2016 Variation of shock-spacing during screech stage-jumps. *Intl J. Aeroacoust.* **15** (3), 324–335.

DAVIES, M. & OLDFIELD, D. 1962 Tones from a choked axisymmetric jet. *Acustica* **12**, 257–277.

EDGINGTON-MITCHELL, D. 2019 Aeroacoustic resonance and self-excitation in screeching and impinging supersonic jets–a review. *Intl J. Aeroacoust.* **18** (2–3), 118–188.

EDGINGTON-MITCHELL, D., HONNERY, D.R. & SORIA, J. 2015 Staging behaviour in screeching elliptical jets. *Intl J. Aeroacoust.* **14** (7), 1005–1024.

EDGINGTON-MITCHELL, D., JAUNET, V., JORDAN, P., TOWNE, A., SORIA, J. & HONNERY, D. 2018 Upstream-travelling acoustic jet modes as a closure mechanism for screech. *J. Fluid Mech.* **855**, R1.

EDGINGTON-MITCHELL, D., WANG, T., NOGUEIRA, P., SCHMIDT, O., JAUNET, V., DUKE, D., JORDAN, P. & TOWNE, A. 2021*a* Waves in screeching jets. *J. Fluid Mech.* **913**, A7.

EDGINGTON-MITCHELL, D., WEIGHTMAN, J., LOCK, S., KIRBY, R., NAIR, V., SORIA, J. & HONNERY, D. 2021*b* The generation of screech tones by shock leakage. *J. Fluid Mech.* **908**, A46.

GAO, J.H. & LI, X.D. 2010 A multi-mode screech frequency prediction formula for circular supersonic jets. *J. Acoust. Soc. Am.* **127** (3), 1251–1257.

GOJON, R. & BOGEY, C. 2017 Flow structure oscillations and tone production in underexpanded impinging round jets. *AIAA J.* **55** (6), 1792–1805.

GOJON, R., BOGEY, C. & MIHAESCU, M. 2018 Oscillation modes in screeching jets. *AIAA J.* **56** (7), 1–7.

GOJON, R., GUTMARK, E. & MIHAESCU, M. 2019 Antisymmetric oscillation modes in rectangular screeching jets. *AIAA J.* **57** (8), 3422–3441.

KNAST, T., BELL, G., WONG, M., LEB, C.M., SORIA, J., HONNERY, D.R. & EDGINGTON-MITCHELL, D. 2018 Coupling modes of an underexpanded twin axisymmetric jet. *AIAA J.* **56** (9), 3524–3535.

LI, X., LIU, N., HAO, P., ZHANG, X. & HE, F. 2021 Screech feedback loop and mode staging process of axisymmetric underexpanded jets. *Exp. Therm. Fluid Sci.* **122**, 110323.

LIN, D. & POWELL, A. 1997 Symmetrical oscillation modes in choked-jet edge tones and screech from rectangular nozzles. *J. Acoust. Soc. Am.* **102** (2), 1235–1238.

MANCINELLI, M., JAUNET, V., JORDAN, P. & TOWNE, A. 2019 Screech-tone prediction using upstream-travelling jet modes. *Exp. Fluids* **60** (1), 22.

MANCINELLI, M., JAUNET, V., JORDAN, P. & TOWNE, A. 2021 A complex-valued resonance model for axisymmetric screech tones in supersonic jets. *J. Fluid Mech.* **928**, A32.

MANNING, T. & LELE, S. 2000 A numerical investigation of sound generation in supersonic jet screech. In *21st AIAA Aeroacoustics Conference. AIAA Paper* 2000-2081.

MERCIER, B., CASTELAIN, T. & BAILLY, C. 2017 Experimental characterisation of the screech feedback loop in underexpanded round jets. *J. Fluid Mech.* **824**, 202–229.

NOGUEIRA, P.A.S. & EDGINGTON-MITCHELL, D.M. 2021 Investigation of supersonic twin-jet coupling using spatial linear stability analysis. *J. Fluid Mech.* **918**, A38.

NOGUEIRA, P.A.S., JAUNET, V., MANCINELLI, M., JORDAN, P. & EDGINGTON-MITCHELL, D. 2022*a* Closure mechanism of the A1 and A2 modes in jet screech. *J. Fluid Mech.* **936**, A10.

NOGUEIRA, P.A.S., JORDAN, P., JAUNET, V., CAVALIERI, A.V.G., TOWNE, A. & EDGINGTON-MITCHELL, D. 2022*b* Absolute instability in shock-containing jets. *J. Fluid Mech.* **930**, A10.

NORUM, T.D. 1983 Screech suppression in supersonic jets. *AIAA J.* **21** (2), 235–240.

PANDA, J. 1999 An experimental investigation of screech noise generation. *J. Fluid Mech.* **378**, 71–96.

PANDA, J., RAMAN, G., ZAMAN, K.B.M.Q., PANDA, J., RAMAN, G. & ZAMAN, K. 1997 Underexpanded screeching jets from circular, rectangular and elliptic nozzles. In *3rd AIAA/CEAS Aeroacoustics Conference, AIAA Paper* 97-1623.

POLDERVAART, L.J., VINK, A.T. & WIJNANDS, A.P.J. 1968 The photographic evidence of the feedback loop of a two dimensional screeching supersonic jet of air. In *Proceedings of the 6th International Congress on Acoustics, Tokyo, Japan.*

PONTON, M.K. & SEINER, J.M. 1992 The effects of nozzle exit lip thickness on plume resonance. *J. Sound Vib.* **154** (3), 531–549.

POWELL, A. 1953 The noise of choked jets. *J. Acoust. Soc. Am.* **25** (3), 385–389.

RAMAN, G. 1997 Cessation of screech in underexpanded jets. *J. Fluid Mech.* **336**, 69–90.

RAMAN, G. & RICE, E.J. 1994 Instability modes excited by natural screech tones in a supersonic rectangular jet. *Phys. Fluids* **6** (12), 3999–4008.

RAO, A.N., KUSHARI, A. & CHANDRA MANDAL, A. 2020 Screech characteristics of under-expanded high aspect ratio elliptic jet. *Phys. Fluids* **32** (7), 076106.

SCHMID, P.J. 2010 Dynamic mode decomposition of numerical and experimental data. *J. Fluid Mech.* **656**, 5–28.

SEMLITSCH, B., MALLA, B., GUTMARK, E.J. & MIHĂESCU, M. 2020 The generation mechanism of higher screech tone harmonics in supersonic jets. *J. Fluid Mech.* **893**, A9.

SHARIFF, K. & MANNING, T.A. 2013 A ray tracing study of shock leakage in a model supersonic jet. *Phys. Fluids* **25** (7), 076103.

SHEN, H. & TAM, C. 2002 Three-dimensional numerical simulation of the jet screech phenomenon. *AIAA J.* **40**, 33–41.

STAVROPOULOS, M., MANCINELLI, M., JORDAN, P., JAUNET, V., EDGINGTON-MITCHELL, D. & NOGUEIRA, P. 2021 Understanding twin-jet screech using a vortex-sheet model. *AIAA Aviation 2021 Forum. AIAA Paper* 2021-2249

SUZUKI, T. & LELE, S.K. 2003 Shock leakage through an unsteady vortex-laden mixing layer: application to jet screech. *J. Fluid Mech.* **490**, 139–167.

TAM, C.K.W., SEINER, J.M. & YU, J.C. 1986 Proposed relationship between broadband shock associated noise and screech tones. *J. Sound Vib.* **110** (2), 309–321.

TAM, C.K.W. & HU, F.Q. 1989 On the three families of instability waves of high-speed jets. *J. Fluid Mech.* **201**, 447–483.

TAM, C.K.W. & TANNA, H.K. 1982 Shock associated noise of supersonic jets from convergent-divergent nozzles. *J. Sound Vib.* **81** (3), 337–358.

TOWNE, A., CAVALIERI, A.V.G., JORDAN, P., COLONIUS, T., SCHMIDT, O., JAUNET, V. & BRÈS, G.A. 2017 Acoustic resonance in the potential core of subsonic jets. *J. Fluid Mech.* **825**, 1113–1152.

TOWNE, A., SCHMIDT, O.T. & COLONIUS, T. 2018 Spectral proper orthogonal decomposition and its relationship to dynamic mode decomposition and resolvent analysis. *J. Fluid Mech.* **847**, 821–867.

WEIGHTMAN, J.L., AMILI, O., HONNERY, D., EDGINGTON-MITCHELL, D. & SORIA, J. 2019 Nozzle external geometry as a boundary condition for the azimuthal mode selection in an impinging underexpanded jet. *J. Fluid Mech.* **862**, 421–448.

WELCH, P. 1967 The use of fast fourier transform for the estimation of power spectra: a method based on time averaging over short, modified periodograms. *IEEE Trans. Audio Electroacoust.* **15** (2), 70–73.

WESTLEY, R. & WOOLLEY, J. 1975 The near field sound pressures of a choked jet when oscillating in the spinning mode. In *2nd Aeroacoustics Conference, AIAA Paper* 1975-479.

WILLERT, C., STASICKI, B., KLINNER, J. & MOESSNER, S. 2010 Pulsed operation of high-power light emitting diodes for imaging flow velocimetry. *Meas. Sci. Technol.* **21** (7), 075402.

ZAMAN, K.B.M.Q. 1995 Spreading characteristics and thrust of jets from asymmetric nozzles. In *34th Aerospace Sciences Meeting and Exhibit, AIAA Paper* 1996-200.